

# Constant bottom water flow into the Indian Ocean for the past 140 ka indicated by sediment Pa/Th ratios

# Constant bottom water flow into the Indian Ocean for the past 140 ka indicated by sediment $^{231}Pa/^{230}Th$ ratios

Alexander L. Thomas,[1] Gideon M. Henderson,[1] and I. Nicholas McCave[2]

Received 10 January 2007; revised 24 April 2007; accepted 21 June 2007; published 15 November 2007.

[1] A down-core $^{231}Pa/^{230}Th$ record has been measured from the southwestern Indian Ocean to reconstruct the history of deep water flow into this basin over the last glacial-interglacial cycle. The $(^{231}Pa_{xs}/^{230}Th_{xs})^0$ ratio throughout the record is nearly constant at approximately 0.055, significantly lower than the production ratio of 0.093, indicating that the proxy is sensitive to changes in circulation and/or sediment flux at this site. The consistent value suggests that there has been no change in the inflow of Antarctic Bottom Water to the Indian Ocean during the last 140 ka, in contrast to the changes in deep circulation thought to occur in other ocean basins. The stability of the $(^{231}Pa_{xs}/^{230}Th_{xs})^0$ value in the record contrasts with an existing sortable silt ($\overline{SS}$) record from the same core. The observed $\overline{SS}$ variability is attributed to a local geostrophic effect amplifying small changes in circulation. A record of authigenic U from the same core suggests that there was reduced oxygen in bottom waters at the core locality during glacial periods. The consistency of the $(^{231}Pa_{xs}/^{230}Th_{xs})^0$ record implies that this could not have arisen by local changes in productivity, thus suggesting a far-field control: either globally reduced bottom water oxygenation or increased productivity south of the Opal Belt during glacials.

**Citation:** Thomas, A. L., G. M. Henderson, and I. N. McCave (2007), Constant bottom water flow into the Indian Ocean for the past 140 ka indicated by sediment $^{231}Pa/^{230}Th$ ratios, *Paleoceanography*, *22*, PA4210, doi:10.1029/2007PA001415.

## 1. Introduction

[2] $(^{231}Pa_{xs}/^{230}Th_{xs})^0$ is a potentially powerful tool for paleoceanographers [e.g., *Henderson and Anderson*, 2003]. Studies in the Atlantic [*Gherardi et al.*, 2005; *McManus et al.*, 2004; *Yu et al.*, 1996] have shown it to be a useful proxy for circulation, and in the Southern Ocean for productivity [*Anderson et al.*, 1998; *Kumar et al.*, 1995] and/or particle type [*Chase et al.*, 2002]. In this study, the temporal and spatial data coverage of $(^{231}Pa_{xs}/^{230}Th_{xs})^0$ in the Indian Ocean is extended, and the ratio used to provide a record of the rate of past deep water flow into the Indian Ocean from the Southern Ocean.

[3] $^{231}Pa$ and $^{230}Th$ are produced in seawater from the in situ decay of $^{235}U$ and $^{234}U$, respectively. Because of the conservative behavior and the long residence time of U, the production, $\beta$, of $^{231}Pa$ and $^{230}Th$ can be assumed to be constant at $\beta_{Pa} = 2.45 \times 10^{-3}$ and $\beta_{Th} = 2.62 \times 10^{-2}$ disintegrations per minute (dpm) $m^{-3}$ $a^{-1}$, leading to a constant production activity ratio of 0.093. Both $^{231}Pa$ and $^{230}Th$ are reversibly scavenged from the dissolved phase onto sinking particles resulting in short oceanic residence times ($t_{res}$), and concentrations that typically increase with depth [*Anderson et al.*, 1983]. Because $t_{res;Pa}$ is longer than $t_{res;Th}$ (120 versus 20 a [*Henderson and Anderson*, 2003]), marked fractionation away from the production ratio can occur within the oceans. In regions of deep water formation such as the North Atlantic, the concentrations of both $^{231}Pa$ and $^{230}Th$ are low because of the convection of low-concentration surface water to depth. Because $^{230}Th$ is more readily scavenged onto sinking particles, the $(^{231}Pa_{xs}/^{230}Th_{xs})^0$ scavenged from seawater to the underlying sediment in such regions is typically less than the production ratio. The preferential removal of $^{230}Th$ results in an increase in the water's $^{231}Pa/^{230}Th$ as the water mass ages, a process which will continue until the output of $^{231}Pa$ and $^{230}Th$ to the sediments occurs at the production ratio (i.e., 0.093). It is the disequilibrium seen in regions of deep water formation and flow that provides the potential of this proxy for assessment of past ocean circulation. The closer to the production ratio that the sediment ($^{231}Pa/^{230}Th$) is, the longer it is since that water left the surface (or had disequilibrium imposed in some other way).

[4] The $^{231}Pa/^{230}Th$ ratio captured in marine sediments therefore may allow the reconstruction of past rates of ocean circulation. If the ratio measured in sediments is to be used in such a way it must first be corrected for the presence of detrital and authigenic $^{231}Pa$ and $^{230}Th$, to give only the "excess" $^{231}Pa$ and $^{230}Th$ scavenged from seawater (see section 4). The $^{231}Pa_{xs}$ and $^{230}Th_{xs}$ must also be corrected for decay since deposition to yield $(^{231}Pa_{xs}/^{230}Th_{xs})^0$ ratios.

[5] $(^{231}Pa_{xs}/^{230}Th_{xs})^0$ in sediment has been used in the North Atlantic [*Gherardi et al.*, 2005; *McManus et al.*, 2004; *Hall et al.*, 2006] to investigate the rate of North Atlantic meridional overturning circulation. These studies have been some of the first to investigate the rate of flow in that region, rather than the pattern of water masses deduced from tracers such as $\delta^{13}C$ [*Duplessy et al.*, 1984] and Cd/Ca

[1]Department of Earth Science, University of Oxford, Oxford, UK.
[2]Department of Earth Science, University of Cambridge, Cambridge, UK.


0883-8305/07/2007PA001415$12.00

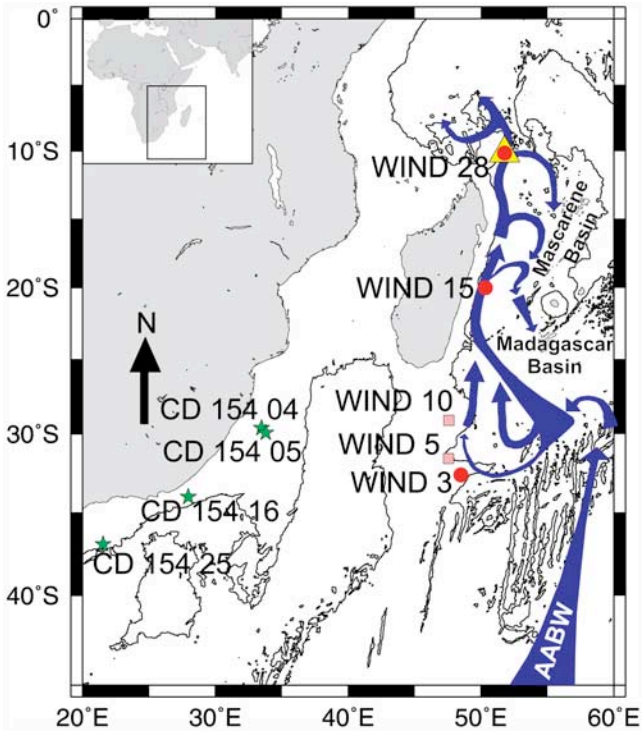


**Figure 1.** A map showing the localities of sediment samples measured in this study. Box core sediment surface scrapes from RRS *Charles Darwin* cruise CD 129 (circles) and Kasten core WIND 28K (triangle) are shown along with core top scrapes from RRS *Charles Darwin* cruise CD 154 (stars). Localities WIND 5 and 10 shown in Figure 2 are shown as squares. The path of Antarctic Bottom Water adapted from *McCave et al.* [2005] is illustrated. The 4000 m isobath is also shown as a thin black line to illustrate the isolation at depth of the Madagascar and Mascarene Basins.

[*Boyle*, 1986]. This early application of $(^{231}Pa_{xs}/^{230}Th_{xs})^0$ has indicated dramatic changes in circulation rate at millennial timescales during deglaciation [*Gherardi et al.*, 2005; *McManus et al.*, 2004] but little change in flow rate between glacial and interglacial times [*Marchal et al.*, 2000; *Yu et al.*, 1996]. No comparable record exists for regions in the Southern Hemisphere, partly because the controls on sedimentary $(^{231}Pa_{xs}/^{230}Th_{xs})^0$ are less clear in the south, reflecting more complex oceanography. Recently, however, *Thomas et al.* [2006] demonstrated, on the basis of water column measurements and a simple model, that sedimentary $(^{231}Pa_{xs}/^{230}Th_{xs})^0$ records from the deep western boundary current region of the Indian Ocean should be controlled by changes in the flow rate of Antarctic Bottom (AABW) into the deep Indian Ocean, rather than the integrated flow of the whole water column. This finding allows investigations of changes in Southern Hemisphere ocean circulation rate to compliment those in the Northern Hemisphere.

## 2. Regional Setting and Samples

[6] The deep Madagascar and Mascarene Basins are filled today from the south by AABW, which overflows the Southwest Indian Ridge [*Toole and Warren*, 1993] and forms a deep western boundary current along the eastern margin of Madagascar (Figure 1). This water mass is not "true" AABW [*Orsi et al.*, 1999] because it has been somewhat altered by mixing in the Antarctic Circumpolar Current, and might more properly be called Lower Circumpolar Deep Water. However, for consistency with previous literature, the term AABW is used in this study to refer to bottom water which is sourced in the Southern Ocean. This boundary current flows north through the basins and exits through the Amirante Passage into the Somali Basin of the northern Indian Ocean. Directly overlying this water mass in the more southerly Madagascar Basin is water derived from the North Atlantic Deep Water (NADW) with a characteristic high salinity. In the northerly Mascarene Basin the overlying water mass, North Indian Deep Water (NIDW), is similar to this NADW derived water, except that it is more enriched in phosphate accumulated during recirculation from the northeastern Indian Ocean [*Sirinvasan et al.*, 2004]. Antarctic Intermediate Water, AAIW, enters the Indian Ocean from the south and overlies both the Atlantic and Indian deep waters. The uppermost water mass, Indian Central Water, is formed within the Indian Ocean's gyres and is characteristically warm and salty. Further details of the oceanography of this region and, in particular the $^{231}Pa$ and $^{230}Th$ in these water masses, are provided by *Thomas et al.* [2006].

[7] A 6 m Kasten core, collected during RRS *Charles Darwin* cruise CD129, was sampled to provide a temporal record of $(^{231}Pa_{xs}/^{230}Th_{xs})^0$. This core, WIND 28K, was taken at 51°46′E 10°9′S, in 4157 m water depth. The site lies at the foot of a steep scarp below the volcanic Farquahar Ridge capped by atolls. Micaceous, clay-rich sediment is derived from run-off from eastern Madagascar. These form turbidites making up the continental rise. Material eroded from the margin is swept into Amirante Passage, where mud waves occur in calcareous mud consisting of 35–60% $CaCO_3$ [*Johnson et al.*, 1983]. The core sits in the boundary current of northward flowing AABW, overlain by southward flowing NIDW with minimal influence of AAIW. The age model for the core is derived from correlation of the benthic (*C. wuellerstorfi*) $\delta^{18}O$ record to the orbitally tuned reference curve (SPECMAP) of *Martinson et al.* [1987] which it closely matches, and six AMS radiocarbon ages [*McCave et al.*, 2005] The good agreement of the $\delta^{18}O$ record with SPECMAP indicates that this core, with a sedimentation rate around 4 cm $ka^{-1}$, is of sufficient resolution to investigate changes on glacial-interglacial timescales. A down-core record of the sortable silt mean grain size ($\overline{SS}$) [*McCave and Hall*, 2006] has been previously measured on the WIND 28K core [*McCave et al.*, 2005], and exhibited some large deviations in average grain size from a relatively constant background value, suggesting distinct fast excursions in bottom water flow speeds. Seven core top samples, selected from cores taken on cruises CD129 and on the later CD154 (Figure 1) were also analyzed to improve the spatial coverage of sedimentary Pa/Th for this undersampled area of the ocean. This number of sites for these distributed analyses is insufficient to merit significant discussion, but the results

**Table 1.** U, Th, $^{230}$Th, and $^{231}$Pa Concentrations and U Isotopic Composition for Surface Sediments from RRS *Charles Darwin* Cruises 129 (WIND) and 154[a]

| Sample | Latitude, °S | Longitude, °E | Depth, m | ($^{238}$U) | ($^{232}$Th) | (U/Th) | $\delta^{234}$U | $U_{auth}$, ppm | $^{230}Th_{xs}{}^{0}$ | $^{231}Pa_{xs}{}^{0}$ | ($^{231}Pa_{xs}{}^{0}$/$^{230}Th_{xs}{}^{0}$) | $F_w$ g cm$^{-2}$ ka$^{-1}$ |
|---|---|---|---|---|---|---|---|---|---|---|---|---|
| WIND 3B 0-2b | 32.38.65 | 048.29.64 | 3731 | 0.439 ± 0.714 | 0.42 ± 0.01 | 1.041 ± 1.693 | −367.2 ± 8.1 | 0.24 ± 0.72 | 15.5 ± 0.4 | 0.52 ± 0.01 | 0.034 ± 0.001 | 0.71 ± 0.02 |
| WIND 15B 0-2b | 19.59.97 | 050.19.96 | 4629 | 1.47 ± 0.007 | 2.85 ± 0.08 | 0.516 ± 0.015 | 50.8 ± 8.1 | 0.14 ± 0.28 | 19.3 ± 0.6 | 1.09 ± 0.03 | 0.056 ± 0.002 | 0.57 ± 0.02 |
| WIND 28B 0-2b | 10.09.33 | 051.46.22 | 4147 | 0.988 ± 0.01 | 1.83 ± 0.05 | 0.539 ± 0.014 | 50.4 ± 8.1 | 0.13 ± 0.18 | 20.9 ± 0.6 | 1.12 ± 0.02 | 0.054 ± 0.002 | 0.52 ± 0.01 |
| CD154 04-4PK | 29.36.66 | 033.27.77 | 2533 | 0.476 ± 0.006 | 0.75 ± 0.02 | 0.632 ± 0.019 | 25.8 ± 8.1 | 0.12 ± 0.07 | 3.3 ± 0.1 | 0.18 ± 0.01 | 0.056 ± 0.003 | 3.36 ± 0.12 |
| CD154 05-5PK | 29.55.26 | 033.47.53 | 1784 | 0.452 ± 0.012 | 0.77 ± 0.02 | 0.59 ± 0.022 | −7.3 ± 8.1 | 0.09 ± 0.08 | 1.6 ± 0.1 | 0.15 ± 0.01 | 0.096 ± 0.007 | 6.82 ± 0.38 |
| CD154 16-15K | 33.42.07 | 028.14.57 | 3166 | 1.349 ± 0.01 | 1.89 ± 0.05 | 0.714 ± 0.019 | −58.6 ± 8.1 | 0.47 ± 0.18 | 3.9 ± 0.2 | 0.24 ± 0.01 | 0.062 ± 0.004 | 2.82 ± 0.16 |
| CD154 24-25K | 36.57.73 | 021.32.91 | 3417 | 1.334 ± 0.01 | 1.32 ± 0.03 | 1.013 ± 0.027 | 3 ± 8.1 | 0.72 ± 0.13 | 4.8 ± 0.2 | | | 2.27 ± 0.09 |

[a]Latitude and longitude are in degrees, and decimal minutes and water depth are in m. All measurements are reported in dpm g$^{-1}$ except $\delta^{234}$U and authigenic U which are reported in ‰ variation from secular equilibrium and in ppm (weight). $^{230}Th_{xs}{}^{0}$ and $^{231}Pa_{xs}{}^{0}$ are the excess $^{230}$Th and $^{231}$Pa in the sediment corrected for decay since sedimentation and for $^{230}$Th and $^{231}$Pa supported by detrital and authigenic U and corrected for decay. Calculation of $^{230}Th_{xs}{}^{0}$ and $^{231}Pa_{xs}{}^{0}$ is discussed in the text, along with the calculation of the mass accumulation rate, $F_w$.

are presented in Tables 1–2 to secure their presence in the public domain.

## 3. Methods

### 3.1. Radiochemical Method

[8] Sediments were dried, weighed, and dissolved using a sequential acid attack with HF $HNO_3$ and aqua regia. The samples were spiked with a mixed $^{229}$Th and $^{236}$U spike [*Henderson et al.*, 2001] and a $^{233}$Pa spike. The $^{233}$Pa spike was produced through neutron irradiation of $^{232}$Th [*Bourdon et al.*, 1999] followed by separation of $^{233}$Pa by anion exchange chromatography [*Anderson and Fleer*, 1982]. Calibration of the $^{233}$Pa concentration in the spike was performed by addition of a $^{236}$U spike to an aliquot of the $^{233}$Pa spike and measurement of the [$^{233}$U,$^{233}$Pa]/$^{236}$U ratio after waiting 4 months until >95% of the $^{233}$Pa had decayed to $^{233}$U. This approach makes the reasonable assumptions that any difference in the ionization between U and the small remaining amount of Pa is insignificant, and that there is no initial $^{233}$U in the spike. It has the significant advantage over decay-counting calibration that is refers directly to a well-known U spike used to assess the U concentrations in the same samples. Once dissolved, the samples were coprecipitated with 10 mg of Fe, and U, Th and Pa were separated by anion chromatography using the methods described by *Thomas et al.* [2006].

[9] Measurements were made using a Nu Instruments MC-ICP-MS [*Belshaw et al.*, 1998]. U was measured statically with $^{234}$U in an ion counter and $^{238}$U, $^{236}$U, and $^{235}$U in Faraday collectors utilizing standard sample bracketing with CRM-145 to correct for ion counter gain and abundance sensitivity [*Robinson et al.*, 2004]. Th isotopes were measured using a two-step procedure, broadly following that of *Robinson et al.* [2004]. Pa was measured with multiple ion counting channels, with $^{231}$Pa in the central ion counting channel (equipped with an energy filter to improve abundance sensitivity from $^{232}$Th and $^{235}$U tailing) and $^{233}$Pa in a high-mass ion counter. Mass bias was assessed externally by bracketing samples with U standard CRM-145, during which assessment of the gains of the ion counters was also made. Interference from $^{232}ThH^{+}$ and abundance sensitivity from $^{232}$Th was corrected by measuring the $^{232}$Th in the Pa cut of each sample, and bracketing every two samples with measurement of a Th standard with a known $^{232}$Th/$^{230}$Th. This standard measurement allows an assessment of the contribution to masses 233 and 231 due to these two analytical effects. The corrections for $^{232}$ThH are typically <1%, but can approach up to 8% if chemical separation of Pa and Th is poor, while the typical correction for abundance sensitivity is approximately only 0.1%. Measurement of Pa was made within a week of chemical separation to ensure that minimal decay of $^{233}$Pa to $^{233}$U had occurred in case there is any difference in the behavior of Pa and U during ionization in the mass spectrometer.

[10] For a small number of samples analyzed at the beginning of this study, covariance of $^{230}$Th and $^{232}$Th concentrations, and failure of replicate analyses to agree with one another indicated incomplete spike equilibration for Th and Pa. These analyses were discarded and are not discussed here. For all future samples, complete spike

**Table 2.** U, Th, $^{230}$Th, and $^{231}$Pa Concentrations and U Isotopic Composition for Samples From the Down-Core Record at WIND 28K[a]

| Sample | Depth, cm | t ka | (238) | (232) | (U/Th) | $\delta^{234}$U | $U_{auth}$ ppm | $^{230}Th_{xs}{}^{0}$ | $^{231}Pa_{xs}{}^{0}$ | $(^{231}Pa_{xs}/^{230}Th_{xs})^{0}$ | $F_w$, gm$^{-2}$ a$^{-1}$ | $F_a$, cm ka$^{-1}$ | Focusing $F_a/F_w$ |
|---|---|---|---|---|---|---|---|---|---|---|---|---|---|
| WIND 28K 3-4b | 3 | 4.41 | 0.931 ± 0.002 | 1.91 ± 0.01 | 0.488 ± 0.003 | 27.6 ± 0.6 | 0.04 ± 0.18 | 20.8 ± 0.3 | | 0.043 ± 0.003 | 0.53 ± 0.01 | 3.17 | 6.04 |
| WIND 28K 3-4 | 3 | 4.41 | 0.956 ± 0.003 | | | 49.5 ± 5.8 | | | 0.89 ± 0.05 | | | 3.17 | |
| WIND 28K 15-16 | 15 | 7.14 | 0.763 ± 0.002 | 1.47 ± 0.01 | 0.519 ± 0.003 | 50.6 ± 0.6 | 0.08 ± 0.14 | 17.9 ± 0.2 | | | 0.61 ± 0.01 | 3.97 | 6.48 |
| WIND 28K 32-33 | 32 | 10.6 | 0.601 ± 0.002 | 1.12 ± 0.01 | 0.536 ± 0.004 | 51.5 ± 0.6 | 0.08 ± 0.11 | 12.4 ± 0.2 | | | 0.88 ± 0.01 | 4.76 | 5.41 |
| WIND 28K 43-44 | 43 | 12.93 | 0.599 ± 0.017 | 1.14 ± 0.03 | 0.525 ± 0.021 | 37.8 ± 9.5 | 0.07 ± 0.11 | 12.2 ± 0.4 | 0.68 ± 0.03 | 0.056 ± 0.003 | 0.90 ± 0.03 | 4.65 | 5.17 |
| WIND 28K 43-44b | 43 | 12.93 | 0.567 ± 0.015 | 1.08 ± 0.03 | 0.522 ± 0.019 | 39 ± 8.1 | 0.06 ± 0.11 | 11.9 ± 0.4 | 0.66 ± 0.01 | 0.055 ± 0.002 | 0.92 ± 0.03 | 4.65 | 5.04 |
| WIND 28K 51-52 | 51 | 14.66 | 0.611 ± 0.002 | 1.27 ± 0.01 | 0.479 ± 0.003 | 30.7 ± 0.6 | 0.02 ± 0.12 | 14.2 ± 0.2 | | | 0.77 ± 0.01 | 4.55 | 5.88 |
| WIND 28K 63-64b | 63 | 17.54 | 0.663 ± 0.003 | 1.52 ± 0.01 | 0.437 ± 0.003 | 23.2 ± 0.6 | −0.05 ± 0.15 | 14.5 ± 0.3 | | 0.046 ± 0.002 | 0.75 ± 0.01 | 3.92 | 5.21 |
| WIND 28K 63-64 | 63 | 17.54 | 0.642 ± 0.004 | | | 37.6 ± 5.8 | | | 0.67 ± 0.03 | | | 3.92 | |
| WIND 28K 93-94 | 93 | 23.0 | 0.499 ± 0.003 | 1.21 ± 0.01 | 0.413 ± 0.003 | 12.6 ± 0.6 | −0.06 ± 0.12 | 11.8 ± 0.2 | | | 0.93 ± 0.02 | 5.56 | 5.98 |
| WIND 28K 119-120 | 119 | 29.9 | 1.822 ± 0.009 | 1.13 ± 0.03 | 1.617 ± 0.040 | 112.6 ± 7.4 | 1.3 ± 0.11 | 12.9 ± 0.4 | 0.72 ± 0.03 | 0.056 ± 0.003 | 0.85 ± 0.03 | 3.6 | 4.23 |
| WIND 28K 119-120b | 119 | 29.9 | 1.951 ± 0.006 | 1.18 ± 0.03 | 1.649 ± 0.045 | 105.5 ± 6.4 | 1.4 ± 0.12 | 13.8 ± 0.5 | 0.79 ± 0.02 | 0.057 ± 0.002 | 0.79 ± 0.03 | 3.6 | 4.55 |
| WIND 28K 157-158 | 157 | 37.37 | 1.001 ± 0.006 | 1.50 ± 0.01 | 0.666 ± 0.006 | 60.6 ± 0.6 | 0.3 ± 0.15 | 18.2 ± 0.3 | | | 0.60 ± 0.01 | 5.19 | 8.65 |
| WIND 28K 171-172 | 171 | 40.1 | 0.509 ± 0.003 | | | 44.2 ± 5.8 | | | 0.56 ± 0.03 | | | 5.13 | |
| WIND 28K 215-216 | 215 | 48.65 | 0.534 ± 0.013 | 0.95 ± 0.02 | 0.559 ± 0.020 | 34.6 ± 7.4 | 0.09 ± 0.09 | 11.7 ± 0.4 | 0.62 ± 0.02 | 0.053 ± 0.003 | 0.93 ± 0.03 | 5.13 | 5.49 |
| WIND 28K 271-272a | 271 | 59.53 | 0.720 ± 0.003 | 1.14 ± 0.04 | 0.634 ± 0.021 | 63.4 ± 4.7 | 0.19 ± 0.11 | 12.5 ± 0.6 | 0.67 ± 0.03 | 0.053 ± 0.003 | 0.88 ± 0.04 | 5.19 | 5.92 |
| WIND 28K 271-272b | 271 | 59.53 | 0.723 ± 0.002 | 1.10 ± 0.03 | 0.660 ± 0.019 | 69.5 ± 4.7 | 0.21 ± 0.11 | 12.6 ± 0.5 | 0.71 ± 0.03 | 0.056 ± 0.003 | 0.87 ± 0.03 | 5.19 | 6.0 |
| WIND 28K 287-288 | 287 | 63.73 | 0.721 ± 0.013 | 1.53 ± 0.04 | 0.472 ± 0.015 | 26.9 ± 7.4 | 0.01 ± 0.15 | 18.4 ± 0.6 | 0.90 ± 0.04 | 0.049 ± 0.003 | 0.59 ± 0.02 | 3.39 | 5.71 |
| WIND 28K 287-288b | 287 | 63.73 | 0.730 ± 0.017 | 1.54 ± 0.04 | 0.474 ± 0.016 | −8.8 ± 8.1 | 0.01 ± 0.15 | 18.3 ± 0.6 | 0.92 ± 0.04 | 0.050 ± 0.003 | 0.60 ± 0.02 | 3.39 | 5.66 |
| WIND 28k 303-304 | 303 | 68.41 | 0.813 ± 0.002 | 1.79 ± 0.07 | 0.455 ± 0.018 | −8.8 ± 4.7 | −0.02 ± 0.18 | 20.1 ± 1.0 | 1.05 ± 0.06 | 0.052 ± 0.004 | 0.54 ± 0.03 | 3.42 | 6.28 |
| WIND 28K 331-332 | 331 | 76.62 | 0.586 ± 0.03 | 1.27 ± 0.03 | 0.461 ± 0.026 | 4.9 ± 7.4 | −0.01 ± 0.13 | 16.0 ± 0.6 | 0.82 ± 0.05 | 0.051 ± 0.003 | 0.69 ± 0.02 | 3.39 | 4.95 |
| WIND 28K 355-356a | 355 | 85.09 | 0.757 ± 0.002 | 1.63 ± 0.05 | 0.463 ± 0.013 | −32.9 ± 4.7 | −0.01 ± 0.16 | 20.3 ± 0.8 | 1.14 ± 0.07 | 0.056 ± 0.004 | 0.54 ± 0.02 | 2.56 | 4.77 |
| WIND 28K 355-356b | 355 | 85.09 | 0.740 ± 0.023 | 1.71 ± 0.04 | 0.432 ± 0.018 | 1.7 ± 9.5 | −0.06 ± 0.17 | 22.6 ± 0.8 | | | 0.48 ± 0.02 | 2.56 | 5.3 |
| WIND 28K 367-368 | 367 | 89.76 | 0.66 ± 0.01 | 1.48 ± 0.04 | 0.445 ± 0.013 | −38.7 ± 7.4 | −0.03 ± 0.15 | 19.7 ± 0.8 | 1.06 ± 0.23 | 0.054 ± 0.012 | 0.56 ± 0.02 | 2.56 | 4.61 |
| WIND 28K 387-388 | 387 | 98.23 | 0.590 ± 0.001 | 1.29 ± 0.04 | 0.458 ± 0.013 | −30.9 ± 4.7 | −0.01 ± 0.13 | 17.2 ± 0.7 | 1.03 ± 0.07 | 0.060 ± 0.005 | 0.64 ± 0.03 | 1.62 | 2.54 |
| WIND 28K 411-412 | 411 | 107.35 | 0.634 ± 0.012 | 1.46 ± 0.04 | 0.435 ± 0.013 | 3.4 ± 7.4 | −0.05 ± 0.14 | 20.5 ± 0.8 | | | 0.53 ± 0.02 | 4.0 | 7.49 |
| WIND 28K 431-432 | 431 | 112.05 | 0.702 ± 0.002 | 1.75 ± 0.05 | 0.402 ± 0.012 | −29.2 ± 4.7 | −0.11 ± 0.17 | 20.9 ± 1.0 | 1.16 ± 0.12 | 0.055 ± 0.006 | 0.52 ± 0.02 | 4.0 | 7.65 |
| WIND 28K 439-440 | 439 | 114.48 | 0.851 ± 0.014 | 2.06 ± 0.05 | 0.412 ± 0.013 | −27.6 ± 8.1 | −0.11 ± 0.2 | 26.4 ± 1.1 | 1.42 ± 0.15 | 0.054 ± 0.006 | 0.41 ± 0.02 | 3.08 | 7.42 |
| WIND 28K 455-456a | 455 | 119.40 | 0.710 ± 0.001 | 1.65 ± 0.05 | 0.430 ± 0.012 | −29.7 ± 4.7 | −0.06 ± 0.16 | 21.4 ± 1.0 | 1.11 ± 0.13 | 0.052 ± 0.007 | 0.51 ± 0.02 | 3.33 | 6.5 |
| WIND 28K 445-456b | 455 | 119.40 | 0.736 ± 0.020 | 1.67 ± 0.04 | 0.441 ± 0.017 | −41.6 ± 9.5 | −0.04 ± 0.16 | 24.0 ± 1.0 | | | 0.46 ± 0.02 | 3.33 | 7.32 |
| WIND 28K 471-472 | 471 | 123.78 | 0.659 ± 0.011 | 1.59 ± 0.04 | 0.413 ± 0.013 | −16.4 ± 8.1 | −0.09 ± 0.16 | 18.5 ± 0.9 | 0.86 ± 0.14 | 0.047 ± 0.008 | 0.59 ± 0.03 | 4.44 | 7.5 |
| WIND 28K 491-492 | 491 | 128.18 | 0.490 ± 0.001 | 1.09 ± 0.03 | 0.450 ± 0.013 | −30.6 ± 4.7 | −0.02 ± 0.11 | 11.3 ± 0.6 | | | 0.97 ± 0.05 | 4.44 | 4.59 |
| WIND 28K 510-511 | 510 | 132.35 | 0.593 ± 0.005 | 1.58 ± 0.01 | 0.374 ± 0.004 | 49.8 ± 0.6 | −0.15 ± 0.15 | 11.5 ± 0.7 | | | 0.95 ± 0.06 | 4.71 | 4.96 |
| WIND 28K 528-529 | 528 | 137.30 | 1.381 ± 0.006 | 1.24 ± 0.03 | 1.113 ± 0.030 | 149.4 ± 8.1 | 0.80 ± 0.12 | 11.6 ± 0.7 | 0.38 ± 0.15 | 0.033 ± 0.013 | 0.94 ± 0.06 | 2.0 | 2.12 |
| WIND 28K 528-529b | 528 | 137.30 | 1.344 ± 0.016 | 1.21 ± 0.03 | 1.109 ± 0.031 | 136.1 ± 6.4 | 0.78 ± 0.12 | 10.8 ± 0.7 | 0.44 ± 0.15 | 0.04 ± 0.014 | 1.01 ± 0.07 | 2.0 | 1.97 |
| WIND 28K 541-542 | 541 | 144.10 | 2.481 ± 0.023 | 1.29 ± 0.01 | 1.922 ± 0.021 | 109.1 ± 0.6 | 1.88 ± 0.13 | 9.9 ± 0.7 | | | 1.10 ± 0.08 | 2.22 | 2.01 |

[a]For explanation, see Table 1. The age of the samples is derived from $\delta^{18}$O stratigraphy augmented with six AMS radiocarbon dates [*McCave et al.*, 2005].

equilibration was ensured by refluxing overnight in 15 N $HNO_3$ following sample dissolution and subsequent reduction of the volume to incipient dryness before redissolving in 7.5 N $HNO_3$ in preparation for anion exchange.

### 3.2. Sedimentological and Isotopic Method

[11] Sedimentological and isotopic methods are detailed by *McCave et al.* [2005] and given briefly here: Cleaning of the benthic foraminifera *Cibicidoides wuellerstorfi* included oxidation of organic matter with 3% $H_2O_2$ and removal of fine grained carbonate. Oxygen and carbon isotopes were measured on a Micromass SIRA dual inlet mass spectrometer at the Godwin Laboratory in Cambridge, with analytical precision of 0.08‰ for $\delta^{18}O$ and 0.06‰ for $\delta^{13}C$ (using the usual delta notation for isotopic ratios). The fine fraction less than 63 $\mu$m was analyzed for the mean grain size of the nonbiogenic sortable silt fraction (abbreviated as $\overline{SS}$) (10–63 $\mu$m range [*McCave et al.*, 1995b]), with carbonate and biogenic opal removed by 1 M acetic acid and 2 M $Na_2CO_3$ solution at 85°C, respectively. The grain size distribution was measured with a Beckman Multisizer-3 Coulter Counter counting $10^4$ particles using a 200 $\mu$m aperture. The precision of $\overline{SS}$ measurements is ca. 2% [*Bianchi et al.*, 1999], equal to 0.3–0.4 $\mu$m in the records shown here. The core was scanned at 1 cm intervals for spectral color reflectance with a Minolta CM-2022 spectrophotometer. Lightness L* was correlated to measured carbonate to yield a detailed carbonate profile.

## 4. Results

[12] Measured concentrations of $^{238}U$ and $^{232}Th$ range from 0.45–1.95 and 0.4–1.5 dpm $g^{-1}$, respectively (Table 1–2). Corrections for $^{230}Th$ and $^{231}Pa$ associated with detrital and authigenic material are made using equations (1) and (2) [*Henderson and Anderson*, 2003]. These corrections assume that authigenic U is formed at the sediment-water interface at the time of deposition and has the U isotopic composition of seawater; and the detrital material is in secular equilibrium.

$$\begin{aligned} {}^{230}\mathrm{Th}_{xs} = {} & {}^{230}\mathrm{Th}_{meas} - \left\{(\mathrm{U/Th})_{detrital} \times {}^{232}\mathrm{Th}_{meas}\right\} \\ & - \left[{}^{238}\mathrm{U}_{meas} - (\mathrm{U/Th})_{detrital} \times {}^{232}\mathrm{Th}_{meas}\right] \\ & \times \left[\left(1 - e^{-\lambda_{230}t}\right) + \frac{\lambda_{230}}{\lambda_{230} - \lambda_{234}}\left(e^{-\lambda_{230}t} - e^{-\lambda_{234}t}\right)\right. \\ & \left. \cdot \left(\left(\frac{{}^{234}\mathrm{U}}{{}^{238}\mathrm{U}_{init}}\right) - 1\right)\right] \end{aligned} \quad (1)$$

$$\begin{aligned} {}^{231}\mathrm{Pa}_{xs} = {} & {}^{231}\mathrm{Pa}_{meas} - \left\{0.046(\mathrm{U/Th})_{detrital} \times {}^{232}\mathrm{Th}_{meas}\right\} \\ & - \left[0.046\ {}^{238}\mathrm{U}_{meas} - 0.046(\mathrm{U/Th})_{detrital}\right. \\ & \left. \times {}^{232}\mathrm{Th}_{meas}\right]\left[1 - e^{-\lambda_{231}t}\right] \end{aligned} \quad (2)$$

[13] Sediment $^{231}Pa_{xs}$ and $^{230}Th_{xs}$ values are then corrected for decay since sedimentation, giving excess concentrations ranging from 0.15–1.42 and 1.6–26.4 dpm $g^{-1}$ respectively (Table 1–2 and Figure 2). Final $(^{231}Pa_{xs}/^{230}Th_{xs})^0$ values are ≈0.05 (i.e., significantly lower than the production ratio of 0.093) and shows no variation outside analytical uncertainty over the past 140 ka (Table 2 and Figure 2).

[14] Authigenic U [*Anderson et al.*, 1989] is calculated from equations (3) and (4).

$$U_{detrital} = (U/Th)_{detrital} \times {}^{232}\mathrm{Th}_{meas} \quad (3)$$

and

$$U_{authigenic} = U_{total} - U_{derital} \quad (4)$$

[15] $U_{auth}$ is rather constant during the past 140 ka at a value close to zero (Figure 2) except for the presence of two distinct peaks to values of ~1.5 ppm, at around 30 and 144 ka, corresponding to glacial periods.

[16] The appropriate value for $(U/Th)_{detrital}$ in equations (1)–(4) is derived from the measured samples on the basis of their $\delta^{234}U$ values. Detrital sediments are expected to have $\delta^{234}U$ close to zero (or possibly slightly negative because of recoil of $^{234}U$). On the other hand, authigenic U should have an initial $\delta^{234}U$ similar to the seawater from which it formed, i.e., 146. Twenty three of the 36 samples measured have a $\delta^{234}U < 50$ and a (U/Th) ratio between 0.4 and 0.5. A value of 0.45 ± 0.05 is therefore chosen as the $(U/Th)_{detrital}$ value for this study. This method of determining $(U/Th)_{detrital}$ has advantages over the basin approach [*Henderson and Anderson*, 2003] or the simple use of an average crustal value [*Anderson*, 1982], because it is specific to an individual core and has a smaller uncertainty, which becomes significant for older samples.

[17] Sediment mass accumulation rate ($F_w$, $gm^{-2}a^{-1}$) is calculated by inverting the measured sedimentary $^{230}Th^0_{xs}$ (equation (5)), assuming a constant flux of $^{230}Th$ from the water column [*Francois et al.*, 2004],

$$F_w = \frac{z(^{234}U)\lambda_{230}}{^{230}\mathrm{Th}^0_{xs}} \quad (5)$$

where $z$ is water depth in m, $(^{234}U)$ is the activity of $^{234}U$ in seawater in dpm $m^{-3}$, and $\lambda_{230}$ is the decay constant of $^{230}Th$ in $a^{-1}$. $F_w$ varies between 0.4 and 1.2 g $m^{-2}$ $ka^{-1}$ (Table 2 and Figure 2). $F_w$ shows significant variation, which appears correlated with benthic $\delta^{18}O$, although with a lag of ≈5–10 ka. $F_w$ also generally correlates with $\%CaCO_3$ (although some of the larger changes in $F_w$ do not have associated changes in $\%CaCO_3$).

[18] Because the $(^{231}Pa_{xs}/^{230}Th_{xs})^0$ record is invariant, changes observed in the $^{230}Th$-normalised mass accumulation rate (Figure 2e) can only be attributed to changes in the particle flux to the seabed of a particle type that does not strongly fractionate $^{231}Pa$ from $^{230}Th$, or to variations in seafloor dissolution of carbonate. Because sinking organic matter and carbonate particles found at this site do fractionate Th from Pa [*Chase et al.*, 2002] it is more likely that the changes in mass accumulation rate are the product of seafloor dissolution than variable productivity. Percent calcite in the sediment (Figure 2f) covaries with mass

accumulation. Dissolution of carbonate, however, cannot explain all of the variation in mass accumulation; particularly the large drop in mass accumulation at 125 ka, which is not associated with a decrease in wt% calcite.

[19] Sediment focusing, $\Psi$, is calculated from the sedimentation rate, $F_a$, (inferred from the age model in cm $ka^{-1}$) and $F_w$ (converted from g $m^{-2}$ $a^{-1}$to g $cm^{-2}$ $ka^{-1}$ and assuming a constant sediment density of 1 g $cm^{-3}$) (equation (6)). In essence, where more $^{230}$Th is accumulating in sediments than is produced in the overlying water column ($\psi > 1$), then it is assumed to be carried to the core site with sediment from elsewhere. $\psi < 1$ indicates winnowing of sediment from the core location [*Suman and Bacon*, 1989].

$$\psi = \frac{F_a}{F_w} \tag{6}$$

[20] Sediment has been focused at this site throughout the last 140 ka, with sediment focusing factors varying between 2 and 8 (Table 2 and Figure 2). This is unsurprising because the core was recovered from contourite sediments. The variation in focusing does not appear to covary with the sortable silt flow speed proxy or with $(^{231}Pa_{xs}/^{230}Th_{xs})^0$ (Figure 2).

## 5. Discussion

### 5.1. Consistency of AABW Flow Into the Indian Ocean

[21] Bottom water leaving the Southern Ocean, such as the branch of AABW that fills the Indian Ocean and bathes the site studied here, will have characteristically low $(^{231}Pa_{xs}/^{230}Th_{xs})^0$. This is due to the passage of the water through the Opal Belt on its way out of the Southern Ocean [*Thomas et al.*, 2006]. Opal preferentially scavenges Pa relative to Th [*Chase et al.*, 2002; *Siddall et al.*, 2005; *Walter et al.*, 1997], resulting in low water column $(^{231}Pa_{xs}/^{230}Th_{xs})^0$ in AABW, which will gradually rise toward an equilibrium value as the water mass continues to travel northward. This equilibrium will be reached when

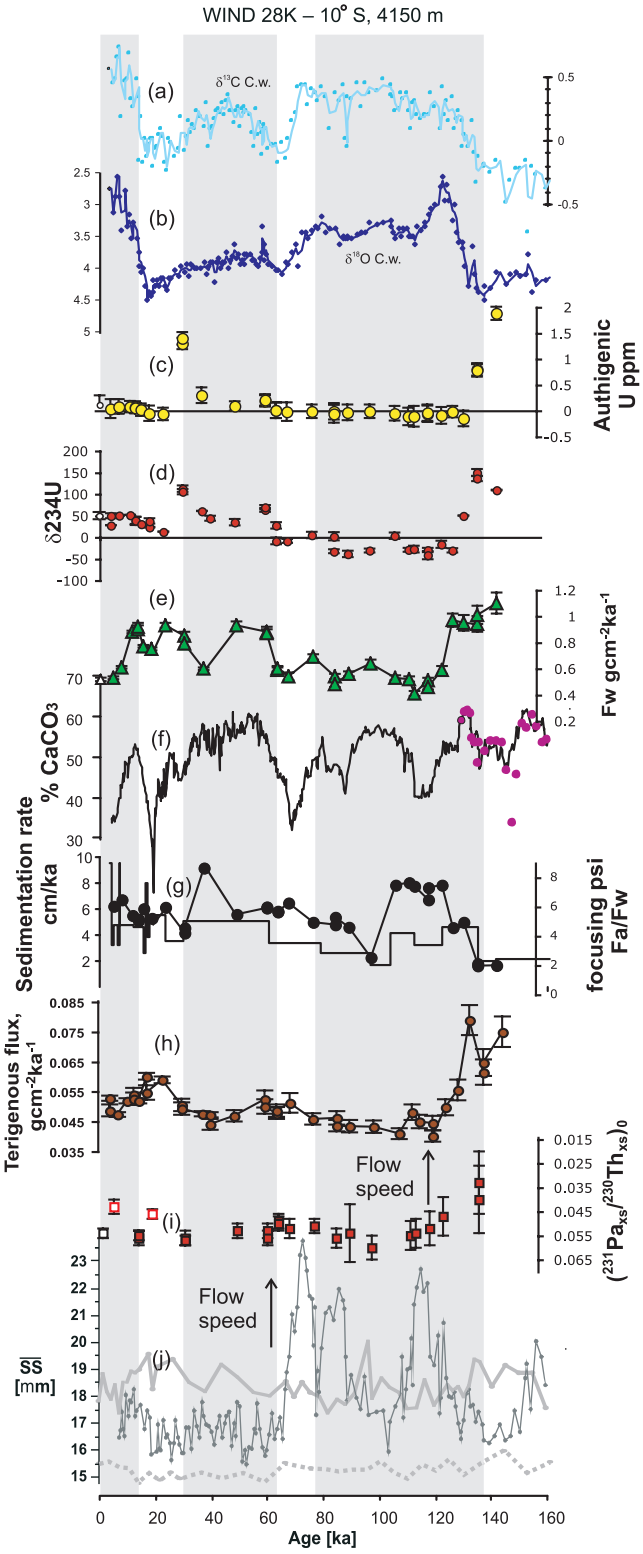


**Figure 2.** (a and b) benthic (*C. wuellerstorfi*) $\delta^{13}$C and $\delta^{18}$O from *McCave et al.* [2005]; (c) authigenic U; (d) $\delta^{234}$U; (e) mass accumulation rate, $F_w$, calculated from measured $^{230}$Th (see text for calculation); (f) %$CaCO_3$ in sediment estimated from the light reflectance: purple dots indicate values of sediment measured for $CaCO_3$ to calibrate the light reflectance (data from T. Keifer, personal communication, 2004); (g) sedimentation rate from the age model of *McCave et al.* [2005] (black line) and sediment focussing derived from the sedimentation and mass accumulation rates; (h) flux of terrigenous to the seabed, calculated from the mass accumulation rate of $^{232}$Th assuming a terrigenous $^{232}$Th concentration of 13 ppm; (i) $(^{231}Pa_{xs}/^{230}Th_{xs})^0$, open red squares representing $(^{231}Pa_{xs}/^{230}Th_{xs})^0$ calculated from $^{231}$Pa and $^{230}$Th measured on different subsamples from the same depth in the core; (j) sortable silt record of WIND 5K 2848 m (dotted light gray line), WIND 10K 3682m (solid light gray line), and WIND 28K 4157 m (solid dark gray line) from *McCave et al.* [2005]. Open black symbols for all plots are values from the core top (0–2 cm) of WIND 28B; a box core reflecting Holocene conditions (C-14 age (*G. sacculifer*) is 5484 a compared with an average of 16 Madagascar-Mascarene Basin core tops of 6793 a).

the export of $^{231}$Pa and $^{230}$Th to sediments is equal to the production ratio (0.093). The expected increase of sedimentary $(^{231}Pa_{xs}/^{230}Th_{xs})^0$ as AABW ages suggests the use of $(^{231}Pa_{xs}/^{230}Th_{xs})^0$ as a proxy for the time since AABW left the Southern Ocean and therefore for the flow rate of AABW. Observed $(^{231}Pa_{xs}/^{230}Th_{xs})^0$ values in the sediment at WIND 28K are below the production ratio indicating that AABW has not yet reached equilibrium and that the proxy should be sensitive to changes in AABW flow at this site.

[22] In more detail, $(^{231}Pa_{xs}/^{230}Th_{xs})^0$ of sediment at a point along the flow path of AABW as it travels northward will be dependent on 4 factors: the initial $(^{231}Pa/^{230}Th)$ of water as it leaves the Opal Belt; the vertical particle flux and type of productivity (opal versus carbonate) between the Opal Belt and the core location; the vertical flux and particle type at the core location; and the flow rate of AABW. The particle flux and type are important because they determine the relative fractionation of $^{231}$Pa and $^{230}$Th. If assumptions can be made about, or constraints placed upon, initial conditions and productivity, then the sedimentary $(^{231}Pa_{xs}/^{230}Th_{xs})^0$ can be used to investigate the northward flow rate of AABW. In this case, given the consistency of the $(^{231}Pa_{xs}/^{230}Th_{xs})^0$ record, the simplest explanation is that all four of these variables have remained constant over the last 140 ka.

[23] It is feasible of course that two or more of the controls on $(^{231}Pa_{xs}/^{230}Th_{xs})^0$ at WIND 28K are varying in such a way that the overall effect is to cancel each other out and thus produce a constant $(^{231}Pa_{xs}/^{230}Th_{xs})^0$. For instance reduced opal productivity in the Southern Ocean would lead to higher $(^{231}Pa_{xs}/^{230}Th_{xs})^0$ at the source, which could be canceled by increased AABW flow speed into the Indian Ocean, providing less time for additional $^{231}$Pa ingrowth. The most likely scenario, however, remains that of no change because a precise covariance between two components of the system is a more complex solution than that of no change. This argument suggests that the flow speed of AABW into the deep Indian Ocean has remained constant for the last 140 ka.

### 5.2. Sensitivity of $(^{231}Pa_{xs}/^{230}Th_{xs})^0$ to Changes in Circulation and Southern Ocean Productivity

[24] To investigate the sensitivity of sedimentary $(^{231}Pa_{xs}/^{230}Th_{xs})^0$ at WIND 28K to changes in circulation, a simple model of water column $^{231}$Pa and $^{230}$Th was used. The model comprises a stack of boxes each 500 m thick, to which initial activities of $^{231}$Pa and $^{230}$Th can be prescribed. Movement of $^{231}$Pa and $^{230}$Th down this water column is achieved through scavenging onto sinking particles, where the distributions of nuclides between the dissolved and particulate phases are described by:

$$Kd^i = A_p^i / \left(A_d^i \times C_p\right), \text{ and } A_t^i = A_p^i + A_d^i \qquad (7)$$

where $A_t^i$, $A_p^i$, and $A_d^i$ are the total, particulate and dissolved activities of nuclide $i$ per unit of seawater; $C_p$ is the concentration of particles; and $Kd^i$ is the partition coefficient for nuclide $i$ onto a particular particle type [*Siddall et al.*, 2005]. $C_p$ is determined by the production of particles in the surface box, which then settle through the water column. Values of *Kd* for carbonate and opal particles are taken from *Siddall et al.* [2005] on the basis of *Chase et al.* [2002].

[25] The activity of nuclides in each box is calculated for each time step, allowing for fluxes in and out from the top and bottom of each box on settling particles and for in situ production from U:

$$ {}^n_j A^i_t = {}^n_{j-1} A^i_t + {}^{n-1}_{j-1} A^i_p \times {}^{n-1}_{j-1} S - {}^n_j A^i_p \times {}^n_j S + {}^n_j \beta^i \qquad (8)$$

where $n$ signifies the box number; $j$ is the time step; $S$ is the proportion of particles from box, $n$, that settle out of the box during a time step, $j$; and $\beta$ is the production of nuclide $i$ in each box during each time step (which is uniform with depth because of the constant U concentration and isotopic composition). Decay of $^{230}$Th and $^{231}$Pa is too slow to be significant relative to the rate of nuclide removal by scavenging and is ignored.

[26] To mimic conditions at our core site with this model, it must be initialised with nuclide concentrations reflecting water that has just left the Southern Ocean. This is achieved in two steps: First a scenario representing the Atlantic Ocean (zero initial activities and a carbonate particle flux of 0.06 $gm^{-2}$ $d^{-1}$, i.e., a typical open ocean particle flux [*Honjo and Manganini*, 1993]) was run to an equilibrium (curve 0c06 in Figure 3); the activity profiles of this run were then used to initialise scenarios representing the Southern Ocean (opal particle fluxes of 0.03, 0.06, and 0.09 $gm^{-2}$ $d^{-1}$). The Southern Ocean scenarios were run for 100 a, in broad agreement with the residence time of water in the Antarctic Circumpolar Current of ~120 a [*Rutberg et al.*, 2000]. These resulting water column profiles are depleted in $^{231}$Pa and enriched in $^{230}$Th, which are in broad agreement with water column measurements form the Southern Ocean [*Rutgers van der Loeff and Berger*, 1993].

[27] In a control calculation, the waters experience scavenging with an opal-rich particle flux of 0.09 $gm^{-2}$ $d^{-1}$ in the Southern Ocean phase and then scavenging with a carbonate particle flux of 0.06 $gm^{-2}$ $d^{-1}$ (i.e., a typical open ocean particle flux [*Honjo and Manganini*, 1993]) to mimic transport northward. This calculation yields a water transport time from the Southern Ocean to the core site of 350 a, based on the observed sediment $(^{231}Pa_{xs}/^{230}Th_{xs})^0$ value of 0.05 at the core site (see curve S100@09c06 in Figure 3). This transport time is in reasonable agreement with the $^{14}$C age difference between Southern Ocean and Indian Ocean [*Andree et al.*, 1986] and with the age difference of a "transient dye tracer" in an ocean GCM [*England*, 1995]. The ±0.01 uncertainty in sedimentary $(^{231}Pa_{xs}/^{230}Th_{xs})^0$ allows water transit times between 260 and 440, equivalent to flow speed variations of ±25%) (Figure 3).

[28] A subsequent set of model calculations were used to assess the sensitivity of $(^{231}Pa_{xs}/^{230}Th_{xs})^0$ at WIND 28K to Southern Ocean productivity by changing the particle fluxes in the Southern Ocean to 0.03, 0.06, 0.09, and 0.12 $gm^{-2}$ $d^{-1}$ (curves Aeqo03, Aeqo06, Aeqo09, and Aeqo12 in Figure 3).

[29] The results of these calculations indicate, as expected, that reduced particle fluxes in the Southern Ocean give rise to elevated $(^{231}Pa_{xs}/^{230}Th_{xs})^0$ leaving the Southern

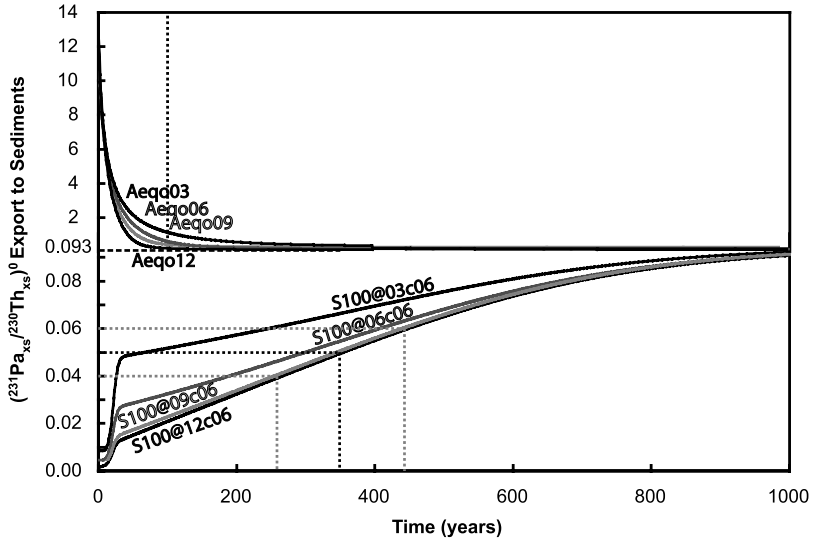


**Figure 3.** Results of model runs showing the $(^{231}Pa_{xs}/^{230}Th_{xs})^0$ exported to sediments, as the model's water "ages" in three hypothetical ocean environments. Note the change in scale on the ordinate axis at the production ratio 0.093 (dashed line). An environment is shown in the upper portion of the graph and simulates conditions in the Southern Ocean where high opal fluxes preferentially scavenge Pa. The initial water column concentrations for this environment are taken from an Atlantic simulation, with zero initial activities, once it has run to equilibrium (e.g., output to sediments = 0.093). The particle flux is then set to 0.03, 0.06, 0.09, and 0.12 $gm^{-2}$ $d^{-1}$ of opal particles with the four curves therefore representing changes in Southern Ocean productivity (curves Aeqo03, Aeqo06, Aeqo09, and Aeqo12). The Indian Ocean model environment is shown in the bottom half of the graph. Initial conditions are taken from each of the four Southern Ocean simulations after 100 a (vertical dotted line, in the upper portion of the figure). The particle flux was set to 0.06 $gm^{-2}$ $d^{-1}$ of carbonate particles (S100@03c06, S100@06c06, S100@09c06, and S100@12c06). The dotted lines indicate the sensitivity of the $(^{231}Pa_{xs}/^{230}Th_{xs})^0$, measured in sediments to changes in circulation "age". In the case presented here the measured range of $(^{231}Pa_{xs}/^{230}Th_{xs})^0$ will allow circulation changes of ±25%. The initially low values of $(^{231}Pa_{xs}/^{230}Th_{xs})^0$ for the Indian Ocean simulations are due to the high concentrations of $^{230}Th$ in Southern Ocean waters due to the low scavenging efficiency of $^{230}Th$ onto opal. This initial $^{230}Th$ excess is rapidly removed from the water column by the high affinity of $^{230}Th$ onto carbonate particles.

Ocean (curves S100@03c06, S100@06c06, S100@09c06, and S100@12c06 in Figure 3). Such reduction in Southern Ocean scavenging could therefore mask faster northward water flow toward the core site and result in no change in sedimentary $(^{231}Pa_{xs}/^{230}Th_{xs})^0$. It is noteworthy, however, that as the particle flux increases, changes in the Southern Ocean $(^{231}Pa_{xs}/^{230}Th_{xs})^0$ become smaller. At the high particle fluxes typically observed in the Southern Ocean (0.16 $gm^{-2}$ $d^{-1}$ [*Honjo et al.*, 2000]), the system is not particularly responsive, so changes in particle fluxes do not greatly affect $(^{231}Pa_{xs}/^{230}Th_{xs})^0$ values, which are then dominated by the flow rate from the Southern Ocean to the core site. This analysis suggests that the constancy of $(^{231}Pa_{xs}/^{230}Th_{xs})^0$ observed does indeed indicate a constancy of northward flow of AABW and cannot be readily explained by coupled productivity and flow rate changes.

### 5.3. Comparison With the Flow Speed Proxy

[30] The $(^{231}Pa_{xs}/^{230}Th_{xs})^0$ record presented here can also be compared to flow rate records from the sortable silt proxy in this and close-by cores. Sortable silt ($\overline{SS}$) is defined as the mean grain size of the 10–63 $\mu$m fraction of the terrigenous component of the sediment [*McCave et al.*, 1995b]. Changing shear stress at the seabed sorts the sediment through winnowing and selective deposition, with higher flow speeds resulting in the deposition of sediment with a coarser $\overline{SS}$. Three peaks in $\overline{SS}$ are observed in the last 140 ka in WIND 28K, at 75, 85, and 115 ka (as well as a fourth at 160 ka) (Figure 2j). These have been interpreted by *McCave et al.* [2005] as possibly caused by increases in flow speed as a result of a local geostrophic effect driven by bottom water density changes. *McCave et al.* [2005] point out that two of these changes correspond to decreases of sea level (inferred from the sea level curve of *Siddall et al.* [2003]) which would lead to a transient increased density contrast between deep waters and the overlying water mass, AABW and NIDW in this case. The second peak in $\overline{SS}$ at 85 ka cannot be directly explained by this mechanism because sea level rises by 40–50 m during the peak of $\overline{SS}$, rather than falling. Two shallower cores from the Madagascar-Mascarene Basin (WIND 5K (3680 m) and WIND 10K (2870 m) [*McCave et al.*, 2005]), show no variation in $\overline{SS}$ (Figure 2j). Thus the geostrophic effect would have to affect current speed only at depths below these cores, perhaps due to amplification by constriction of flow through the Amirante Passage near the site of WIND 28K.

[31] Sedimentary $(^{231}Pa_{xs}/^{230}Th_{xs})^0$ is likely to be "set" by the concentrations of $^{231}Pa$ and $^{230}Th$ in the bottom few hundred meters from the seabed [*Thomas et al.*, 2006]. Thus $\overline{SS}$ and $(^{231}Pa_{xs}/^{230}Th_{xs})^0$ are both proxies for bottom water flow rate, and might be expected to agree with each other,. In detail, however, the two proxies are recording different aspects of the flow. $\overline{SS}$ is a measure of shear stress at the sediment-water interface at the particular site, while $(^{231}Pa_{xs}/^{230}Th_{xs})^0$ is controlled by average flow between the Opal Belt and the core site. The local control of $\overline{SS}$ is illustrated by looking at variation across a bed form, where $\overline{SS}$ varies by large amounts on small scales depending on the position with respect to topography [*McCave et al.*, 1995b]. Different locations can vary greatly in sensitivity to flow changes and consequent effects on $\overline{SS}$. The large variations of $\overline{SS}$ in the Amirante Passage may thus be artifacts of slight variation in the position of the flow. Excepting the spikes, any changes in the "background" $\overline{SS}$ are relatively small [*McCave et al.*, 2005]. A possible reconciliation of the $(^{231}Pa_{xs}/^{230}Th_{xs})^0$ and $\overline{SS}$ data at 28K, therefore, is to invoke a relatively constant flow of AABW as suggested by the $(^{231}Pa_{xs}/^{230}Th_{xs})^0$ record, but the flow into the narrow Amirante Passage was briefly intensified, or its position on the slope altered, due to changes in density contrast caused by falling sea level. Such an explanation is also consistent with the constant SS observed at other sites in the area where flow is not so restricted.

[32] Although the $\overline{SS}$ proxy is also potentially vulnerable to rapid direct input of detrital sediment downslope that is not sorted by the bottom current [*McCave and Hall*, 2006], for instance in turbidity flows, there is no evidence for such input in the vicinity of WIND 28K or for over 100 km upstream. The fact that the spikes in $\overline{SS}$ are seen only at the Amirante Passage site and that the background is nearly constant there and at the southern sites WIND 5K and 10K suggests that the constant $(^{231}Pa_{xs}/^{230}Th_{xs})^0$ ratios below the production ratio indicate that the regional flow of AABW into the Indian Ocean has varied only slightly over the past 140 ka.

### 5.4. Constant AABW Flow Compared to Glacial-Interglacial Changes Elsewhere

[33] In the Atlantic, traditional water mass tracers, such as the Cd/Ca ratio and $\delta^{13}C$ of benthic foraminifera, indicate that during interglacial conditions northern sourced deep water dominates the North Atlantic basins, while during glacials a nutrient-rich southern sourced deep water dominates the Atlantic [*Boyle and Keigwin*, 1982; *Raymo et al.*, 1990]. Radiocarbon measurements in the North Atlantic similarly suggest the dominance of southern sourced waters during glacials, and radiocarbon enriched northern sourced waters following deglaciation [*Robinson et al.*, 2005]. Such data gives rise to a view of deep circulation on glacial-interglacial timescales in which changes in the north are opposite to those in the south.

[34] Sortable silt records provide information about the rate of bottom water flow and also suggest asynchronous behavior in the Northern and Southern hemispheres on orbital timescales. A record from the South Pacific indicates fast flow during glacials [*Hall et al.*, 2001], while one from the Ceara Rise of the equatorial Atlantic [*Groger et al.*, 2003] and others from the NE Atlantic [*Hall and McCave*, 2000; *McCave et al.*, 1995a] record faster flow during interglacials.

[35] In contrast, existing $(^{231}Pa_{xs}/^{230}Th_{xs})^0$ records from the Atlantic seem to disagree with this established view of ocean circulation. The average $(^{231}Pa_{xs}/^{230}Th_{xs})^0$ of North Atlantic glacial age sediments is similar that of Holocene sediments [*Yu et al.*, 1996], indicating similar transport of $^{231}Pa$ to the Southern Ocean [*Marchal et al.*, 2000]. Time series from the North Atlantic [*Gherardi et al.*, 2005; *McManus et al.*, 2004], although exhibiting large millennial-scale variability, also suggest values for the last glacial that are not very different to those for the Holocene.

[36] The WIND 28K record presented here provides a Southern Hemisphere complement to these Northern Hemisphere $(^{231}Pa_{xs}/^{230}Th_{xs})^0$ records. It is notable that, although the record is not of high enough resolution to observe millennial change, the longer-term pattern is one of no change, similar to that seen for in the North Atlantic on orbital timescales. This may suggest little change in the overall rate of flow of deep water masses between glacial and interglacial times, despite the observed changes in water mass distributions.

[37] Perhaps the strongest evidence for changes in the actual flow rate of southern sourced deep water between glacials and interglacials comes from a $\overline{SS}$ record in the southern Pacific Ocean [*Hall et al.*, 2001], which indicates stronger flow during glacial periods. It is however possible that AABW flow history differs from ocean to ocean, with AABW flow into the Pacific varying with time while that into the Indian Ocean does not. AABW that flows into the Indian Ocean is formed in the Weddell Sea, while that which flows into the Pacific is a combination of AABW from the Weddell Sea and that formed on the Adelie Shelf [*Rintoul*, 1998] at approximately 140°E. It also remains possible that variations in the flow of shallower water masses have occurred on glacial-interglacial timescales, but such changes cannot be observed with the $(^{231}Pa_{xs}/^{230}Th_{xs})^0$ proxy in this core as it is situated beneath AABW.

[38] The lack of change in flow rate of AABW on glacial-interglacial timescales has implications for the interpretation of paleowater mass tracers. Authigenic Nd istopes [*Piotrowski et al.*, 2004; *Rutberg et al.*, 2000], along with nutrient proxies such as $\delta^{13}C$ [*Oppo and Fairbanks*, 1987] have been used to investigate the paleodistribution of water masses. These proxies have shown a deglacial trend toward increasing influence of North Atlantic sourced deep waters in the Southern and Pacific oceans. The new $(^{231}Pa_{xs}/^{230}Th_{xs})^0$ constraints presented here suggest that it is the strength of North Atlantic sourced deep waters rather than changes in the Southern Ocean that are responsible for the deglacial changes in water mass distribution.

### 5.5. Authigenic U

[39] For most of the last 140 ka the sedimentary (U/Th) ratio recorded in WIND 28K is constant, and there has been little or no addition of $U_{auth}$. There are, however, two peaks in authigenic uranium at 30 and 140 ka. Authigenic U is formed in sediments which are experiencing reducing

conditions due to a depletion of $O_2$ in the overlying water or to a high flux of organic carbon from the overlying water column [*Anderson et al.*, 1998; *Kumar et al.*, 1995; *Mangini et al.*, 2001]. Peaks in $U_{auth}$ observed in WIND 28K may have initially extended to younger sediment, but been subsequently removed when oxic conditions returned and ''burnt down'' into existing sediment [*Mangini et al.*, 2001].

[40] Changes to higher productivity, at the WIND 28K site, to cause sedimentary anoxia and $U_{auth}$ formation should be recorded as increased sedimentary $(^{231}Pa_{xs}/^{230}Th_{xs})^0$. No such change in $(^{231}Pa_{xs}/^{230}Th_{xs})^0$ is observed in the 30 ka and 140 ka portions of WIND 28K, suggesting that authigenic U production is not controlled by local productivity but by changes in the oxygen concentration of bottom water arriving at the site. This may be due to increased Southern Ocean productivity or may reflect global changes. As discussed in section 5.2, if there were increased productivity in the glacial Southern Ocean [*Abelmann et al.*, 2006], it may not have affected the $^{231}Pa$ and $^{230}Th$ contents of AABW arriving at WIND 28K. Therefore the cause of reduced oxygen concentrations in AABW during glacials cannot be rigorously deduced from this core alone.

[41] The required decrease in oxygenation may also have been caused by a low original oxygen concentration in deep waters entering the Southern Ocean from the Atlantic [*Mangini et al.*, 2001], which should have no effect on the $^{231}Pa$ and $^{230}Th$ contents of AABW leaving the Southern Ocean. It is clear that it is impossible to conclusively resolve these two scenarios from only one core, but a wider geographical distribution of $U_{auth}$ data, coupled with sedimentary $(^{231}Pa_{xs}/^{230}Th_{xs})^0$, will enable the effects of local productivity to be removed and the history of global bottom water oxygen concentration to be deduced.

### 5.6. Detrital Provenance

[42] The $(U/Th)_{detrital}$ presented here provides the first such value for the Indian Ocean. The value of $0.45 \pm 0.05$ is considerably lower than that used in previous studies in the Indian Ocean [*Marcantonio et al.*, 2001; *Pourmand et al.*, 2004] derived from the average crustal value of $0.8 \pm 0.2$ [*Anderson et al.*, 1990; *Taylor*, 1964]. The new value for the Indian Ocean lies within the estimate of $0.4 \pm 0.1$ for the Southern Ocean, south of the Antarctic Polar Front [*Walter et al.*, 1997]. Although the Indian Ocean at WIND 28 appears to have $(U/Th)_{detrital}$ similar to the Southern Ocean, previous studies from north of the Polar Front in the Atlantic sector of the Southern Ocean have indicated higher $(U/Th)_{detrital}$. *Walter et al.* [1997] for instance, found large latitudinal variations within the Southern Ocean with increasing values to the north. So it would therefore be unwise to associate the low $(U/Th)_{detrital}$ observed at 10°S in the Indian Ocean with a Southern Ocean source. With only one measurement of $(U/Th)_{detrital}$ in the Indian Ocean, the possibility of variations in the $(U/Th)_{detrital}$ value within the basin remains a significant possibility.

[43] The constant value of $(U/Th)_{detrital}$ over the last 140 ka suggests that the source of the detrital material remained the same. A compilation of measurements of igneous rocks from Madagascar (B. Sarbas et al., 2006, GEOROC database, http://georoc.mpch-mainz.gwdg.de) yield an average (U/Th) of 0.7 ($\pm 0.2$ $1\sigma$) with only 6% of samples having a (U/Th) < 0.5. It is therefore unlikely that the source of the detrital material is principally from Madagascar unless it is biased toward a highly localized, undersampled, region. The other plausible source of the detrital material to WIND 28K is aeolian dust. Seasonal wind vectors [*da Silva et al.*, 1994] suggest the source of aeolian dust may be from Asia during its winter monsoon or from Australia during its winter monsoon. Although there are no constraints on the compositions of these components, the simplest explanation of the constant data is that the sources of detritus to the sediment, or the balance between the sources, have remained the same during the last 140 ka. There is no evidence of a switch to volcanic source rocks in the glacial at lower sea level when the top of Farquahar Ridge was exposed.

## 6. Conclusions

[44] New measurements of $(^{231}Pa_{xs}/^{230}Th_{xs})^0$ have been made in a western Indian Ocean sediment core a full glacial cycle (140 ka to present). Values of $(^{231}Pa_{xs}/^{230}Th_{xs})_0$ are below the production ratio and are therefore sensitive to changes in circulation and export productivity, but show no significant variation over the past 140 ka. This is most simply explained if both productivity and advection rates of AABW from the Southern Ocean have remained approximately constant during this interval. This is in contrast to the $\overline{SS}$ record in the same core, which indicates periods of increased flow. These two observations can be reconciled because local topographic effects, accelerating the flow into Amirante Passage, may cause the dominant peaks in the $\overline{SS}$ record whereas $(^{231}Pa_{xs}/^{230}Th_{xs})^0$ is affected by advection over a broader region and is therefore more representative of the regional current speed. The ''background'' $\overline{SS}$ values also changes only very slightly between glacial and interglacial both in the studied core and two others further south away from topographic influences, further suggesting no significant change in flow rates of AABW during orbital timescale climate cycles.

[45] The presence of authigenic U in sediments formed during the last two glacial periods indicates reduced oxygen in deep waters at the site during glacial times which cannot be attributed to increased local productivity.

[46] **Acknowledgments.** We wish to thank Nick Belshaw for assistance with mass spectrometry, Sylvain Pichat and Julia Shaw for advice and assistance in the production of $^{233}Pa$ from $^{232}Th$, and Thorsten Kiefer for providing samples of WIND 28K and access to the associated data. We also like to thank two anonymous reviewers for their constructive comments. Alex Thomas was supported by NERC studentship NER/S/A/2002/10531. Cruise CD129 coring and subsequent sediment processing was supported by NERC grant NER/A/S/2000/0493 to I. N. McCave and H. Elderfield.

## References


Abelmann, A., R. Gersonde, G. Cortese, G. Kuhn, and V. Smetacek (2006), Extensive phytoplankton blooms in the Atlantic sector of the glacial Southern Ocean, *Paleoceanography*, *21*, PA1013, doi:10.1029/2005PA001199.

Anderson, R. F. (1982), Concentration, vertical flux, and remineralisation of particulate uranium in seawater, *Geochim. Cosmochim. Acta*, *46*, 1293–1299.

Anderson, R. F., and A. P. Fleer (1982), Determination of natural actinides and plutonium in marine particulate material, *Anal. Chem.*, *54*, 1142–1147.

Anderson, R. F., M. P. Bacon, and P. G. Brewer (1983), Removal of $^{230}$Th and $^{231}$Pa from the open ocean, *Earth Planet. Sci. Lett.*, *62*, 7–23.

Anderson, R. F., M. Q. Fleisher, and A. P. Lehuray (1989), Concentration, oxidation state and, particle flux of uranium in the Black Sea, *Geochim. Cosmochim. Acta*, *53*, 2215–2224.

Anderson, R. F., Y. Lao, W. S. Broecker, S. E. Trumbore, H. J. Hofmann, and W. Wolfli (1990), Boundary scavenging in the Pacific Ocean: A comparison of $^{10}$Be and $^{231}$Pa, *Earth Planet. Sci. Lett.*, *96*, 287–304.

Anderson, R. F., N. Kumar, R. A. Mortlock, P. N. Froelich, P. Kubik, B. Dittrich-Hannen, and M. Suter (1998), Late-Quaternary changes in productivity of the Southern Ocean, *J. Mar. Syst.*, *17*, 497–514.

Andree, M., et al. (1986), Limits on the ventilation rate for the deep ocean over the last 12,000 years, *Clim. Dyn.*, *1*, 53–62.

Belshaw, N. S., P. A. Freedman, R. K. O'Nions, M. Frank, and Y. Guo (1998), A new variable dispersion double-focusing plasma mass spectrometer with performance illustrated for Pb isotopes, *Int. J. Mass Spectrom.*, *181*, 51–58.

Bianchi, G. G., I. R. Hall, I. N. McCave, and L. Joseph (1999), Measurement of the sortable silt current speed proxy using the Sedigraph 5100 and Coulter Multisizer IIe: Precision and accuracy, *Sedimentology*, *46*, 1001–1014.

Bourdon, B., J.-L. Joron, and C. J. Allègre (1999), A method for $^{231}$Pa analysis by thermal ionisation mass spectrometry in silicate rocks, *Chem. Geol.*, *157*, 147–151.

Boyle, E. A. (1986), Paired Cd and $\delta^{13}$C data from benthic foraminifera: Implications for ocean circulation, phosphorus, and atmospheric CO2, *Geochim. Cosmochim. Acta*, *50*, 265–276.

Boyle, E. A., and L. D. Keigwin (1982), Deep circulation of the North-Atlantic over the last 200,000 years: Geochemical evidence, *Science*, *218*, 784–787.

Chase, Z., R. F. Anderson, M. Q. Fleisher, and P. W. Kubik (2002), The influence of particle composition and particle flux on scavenging of Th, Pa and Be in the ocean, *Earth Planet. Sci. Lett.*, *204*, 215–219.

da Silva, A. M., C. C. Young-Molling, and S. Levitus (Eds.) (1994), *Atlas of Surface Marine Data 1994*, vol. 1, *Algorithms and Procedures*, *NOAA Atlas NESDIS*, vol. 6, 83 pp., NOAA, Silver Spring, Md.

Duplessy, J.-C., N. J. Shackleton, R. K. Matthews, W. Prell, W. F. Ruddiman, M. Caralp, and C. H. Hendy (1984), $^{13}$C Record of benthic foraminifera in the last interglacial ocean: implications for the carbon cycle and the global deep water circulation, *Quat. Res.*, *21*, 225–243.

England, M. H. (1995), The age of water and ventilation timescales in a global ocean model, *J. Phys. Oceanogr.*, *25*, 2756–2777.

Francois, R., M. Frank, M. Rutgers Van Der Loeff, and M. P. Bacon (2004), $^{230}$Th normalization: An essential tool for interpreting sedimentary fluxes during the late Quaternary, *Paleoceanography*, *19*, PA1018, doi:10.1029/2003PA000939.

Gherardi, J. M., L. Labeyrie, J. F. Mcmanus, R. Francois, L. C. Skinner, and E. Cortijo (2005), Evidence from the northeastern Atlantic basin for variability in the rate of the meridional overturning circulation through the last deglaciation, *Earth Planet. Sci. Lett.*, *240*, 710–723.

Groger, M., R. Henrich, and T. Bickert (2003), Glacial-interglacial variability in lower North Atlantic Deep Water: Inference from silt grainsize analysis and carbonate preservation in the western equatorial Atlantic, *Mar. Geol.*, *201*, 321–332.

Hall, I. R., and I. N. McCave (2000), Palaeocurrent reconstruction, sediment and thorium focussing on the Iberian margin over the last 140 ka, *Earth Planet. Sci. Lett.*, *178*, 151–164.

Hall, I. R., N. I. McCave, N. J. Shackleton, G. P. Weedon, and S. E. Harris (2001), Intensified deep Pacific inflow and ventilation in Pleistocene glacial times, *Nature*, *412*, 809–812.

Hall, I. R., S. B. Moran, R. Zahn, P. C. Knutz, C. C. Shen, and R. L. Edwards (2006), Accelerated drawdown of meridional overturning in the late-glacial Atlantic triggered by transient pre-H event freshwater perturbation, *Geophys. Res. Lett.*, *33*, L16616, doi:10.1029/2006GL026239.

Henderson, G. M., and R. F. Anderson (2003), The U-series toolbox for paleoceanography, in *Reviews in Mineralogy and Geochemistry "Uranium Series Geochemistry"*, edited by B. Bourdon et al., pp. 493–531, Mineral. Soc. of Am., Washington, D. C.

Henderson, G. M., N. C. Slowey, and M. Q. Fleisher (2001), U-Th dating of carbonate platform and slope sediments, *Geochim. Cosmochim. Acta*, *65*, 2757–2770.

Honjo, S., and S. J. Manganini (1993), Annual biogenic particle fluxes to the interior of the North-Atlantic Ocean: Studied at 34-degrees-N 21-degrees-W and 48-degrees-N 21-degrees-W, *Deep Sea Res., Part II*, *40*, 587–607.

Honjo, S., R. Francois, S. J. Manganini, J. Dymond, and R. Collier (2000), Particle fluxes to the interior of the Southern Ocean in the western Pacific sector along 170°W, *Deep Sea Res., Part II*, *47*, 3521–3548.

Johnson, D. A., M. T. Ledbetter, and J. E. Damuth (1983), Neogene sedimentation and erosion in the Amirante Passage, western Indian Ocean, *Deep Sea Res., Part A*, *30*, 195–219.

Kumar, N., R. F. Anderson, R. A. Mortlock, P. N. Froelich, P. Kubik, H. B. Dittrich, and M. Suter (1995), Increased biological productivity and export production in the glacial Southern Ocean, *Nature*, *378*, 675–680.

Mangini, A., M. Jung, and S. Laukenmann (2001), What do we learn from peaks of uranium and of manganese in deep sea sediments?, *Mar. Geol.*, *177*, 63–78.

Marcantonio, F., R. F. Anderson, S. Higgins, M. Q. Fleisher, M. Stute, and P. Schlosser (2001), Abrupt intensification of the SW Indian Ocean monsoon during the last deglaciation: Constraints from Th, Pa, and He isotopes, *Earth Planet. Sci. Lett.*, *184*, 505–514.

Marchal, O., R. Francois, T. F. Stocker, and F. Joos (2000), Ocean thermohaline circulation and sedimentary $^{231}$Pa/$^{230}$Th ratio, *Paleoceanography*, *15*, 625–641.

Martinson, D. G., N. G. Pisias, J. D. Hays, J. Imbrie, T. C. Moore, and N. J. Shackleton (1987), Age dating and the orbital theory of the ice ages: Development of a high resolution 0 to 300,000-year chronostratigraphy, *Quat. Res.*, *27*, 1–29.

McCave, I. N., and I. R. Hall (2006), Size sorting in marine muds: Processes, pitfalls and prospects for paleoflow-speed proxies, *Geochem. Geophys. Geosyst.*, *7*, Q10N05, doi:10.1029/2006GC001284.

McCave, I. N., T. Kiefer, D. J. R. Thornalley, and H. Elderfield (2005), Deep flow in the Madagascar-Mascarene Basin over the last 150,000 years, *Philos. Trans. R. Soc.*, *363*, 81–99.

McCave, I. N., B. Manighetti, and S. G. Robinson (1995a), Changes in circulation of the North Atlantic during the last 25,000 years inferred from grainsize measurements, *Nature*, *374*, 149–152.

McCave, I. N., B. Manighetti, and S. G. Robinson (1995b), Sortable silt and fine sediment size/composition slicing; parameters for palaeocurrent speed and palaeoceanography, *Paleoceanography*, *10*, 593–610.

McManus, J. F., R. Francois, J.-M. Gherardi, L. Keigwin, and S. Brown-Leger (2004), Collapse and rapid resumption of Atlantic meridional circulation linked to deglacial climate changes, *Nature*, *428*, 834–837.

Oppo, D. W., and R. G. Fairbanks (1987), Variability in the deep and intermediate water circulation of the Atlantic-Ocean during the past 25,000 years: Northern-Hemisphere modulation of the Southern-Ocean, *Earth Planet. Sci. Lett.*, *86*, 1–15.

Orsi, A. H., G. C. Johnson, and J. L. Bullister (1999), Circulation, mixing, and production of Antarctic Bottom Water, *Prog. Oceanogr.*, *43*, 55–109.

Piotrowski, A. M., S. L. Goldstein, S. R. Hemming, and R. G. Fairbanks (2004), Intensification and variability of ocean thermohaline circulation through the last deglaciation, *Earth Planet. Sci. Lett.*, *225*, 205–220.

Pourmand, A., F. Marcantonio, and H. Schulz (2004), Variations in productivity and aeolian fluxes in the northeastern Arabian Sea during the past 110 ka, *Earth Planet. Sci. Lett.*, *221*, 39–54.

Raymo, M. E., W. F. Ruddiman, N. J. Shackleton, and D. W. Oppo (1990), Evolution of Atlantic Pacific delta-C-13 gradients over the last 2.5 My, *Earth Planet. Sci. Lett.*, *97*, 353–368.

Rintoul, S. R. (1998), On the origin and influence of Adelie Land Bottom Water, in *Ocean, Ice, and Atmosphere: Interactions at the Antarctic Continental Margin*, edited by S. S. Jacobs and R. F. Weiss, pp. 151–171.

Robinson, L. F., N. S. Belshaw, and G. M. Henderson (2004), U and Th concentrations and isotope ratios in modern carbonates and waters from the Bahamas, *Geochim. Cosmochim. Acta*, *68*, 1777–1789.

Robinson, L. F., J. F. Adkins, L. D. Keigwin, J. Southon, D. P. Fernandez, S. L. Wang, and D. S. Scheirer (2005), Radiocarbon variability in the western North Atlantic during the last deglaciation, *Science*, *310*, 1469–1473.

Rutberg, R. L., S. R. Hemming, and S. L. Goldstein (2000), Reduced North Atlantic Deep Water flux to the glacial Southern Ocean inferred from neodymium isotope ratios, *Nature*, *405*, 935–938.

Rutgers Van Der Loeff, M. M., and G. W. Berger (1993), Scavenging of $^{230}$Th and $^{231}$Pa near the

Antarctic Polar Front in the South Atlantic, *Deep Sea Res., Part I*, *40*, 339–357.

Siddall, M., E. J. Rohling, A. Almogi-Labin, C. Hemleben, D. Meischner, I. Schmelzer, and D. A. Smeed (2003), Sea-level fluctuations during the last glacial cycle, *Nature*, *423*, 853–858.

Siddall, M., G. M. Henderson, N. R. Edwards, M. Frank, S. A. Muller, T. F. Stocker, and F. Joos (2005), Pa-231/Th-230 fractionation by ocean transport, biogenic particle flux and particle type, *Earth Planet. Sci. Lett.*, *237*, 135–155.

Sirinvasan, A., Z. Top, P. Schlosser, R. Hohmann, M. Iskandarani, D. B. Olson, J. E. Lupton, and W. J. Jenkins (2004), Mantle $^{3}$He distribution and deep circulation in the Indian Ocean, *J. Geophys. Res.*, *109*, C06012, doi:10.1029/2003JC002028.

Suman, D. O., and M. P. Bacon (1989), Variations in Holocene sedimentation in the North American basin determined from $^{230}$Th measurements, *Deep Sea Res., Part A*, *36*, 869–878.

Taylor, S. R. (1964), Abundance of chemical elements in the continental crust: a new table, *Geochim. Cosmochim. Acta*, *28*, 1273–1286.

Thomas, A. L., G. M. Henderson, and L. F. Robinson (2006), Interpretation of the $^{231}$Pa/$^{230}$Th paleocirculation proxy: New water-column measurements from the southwest Indian Ocean, *Earth Planet. Sci. Lett.*, *241*, 493–504.

Toole, J. M., and B. A. Warren (1993), A hydrographic section across the subtropical south Indian Ocean, *Deep Sea Res., Part I*, *40*, 1973–2019.

Waelbroeck, C., C. Levi, J. C. Duplessy, L. Labeyrie, E. Michel, E. Cortijo, F. Bassinot, and F. Guichard (2006), Distant origin of circulation changes in the Indian Ocean during the last deglaciation, *Earth Planet. Sci. Lett.*, *243*, 244–251.

Walter, H. J., M. M. Rutgers Van De Loeff, and H. Hoeltzen (1997), Enhanced scavenging of $^{231}$Pa relative to $^{230}$Th in the South Atlantic south of the Polar Front: Implications for the use of the $^{231}$Pa/$^{230}$Th as a paleoproductivity proxy, *Earth Planet. Sci. Lett.*, *149*, 85–100.

Yu, E. F., R. Francois, and M. P. Bacon (1996), Similar rates of modern and last-glacial ocean thermohaline circulation inferred from radiochemical data, *Nature*, *379*, 689–694.

G. M. Henderson and A. L. Thomas, Department of Earth Science, University of Oxford, Parks Road, Oxford, OX1 3PR, UK. (alext@earth.ox.ac.uk)

I. N. McCave, Department of Earth Science, University of Cambridge, Downing Street, Cambridge, UK.